NUMERICAL ANALYSIS OF PHYSICAL PHENOMENA DURING HARDENING OF STEEL FOR COLD WORK

Tomasz DOMAŃSKI, Wiesława PIEKARSKA, Marcin KUBIAK

Institute of Mechanics and Machine Design, Czestochowa University of Technology, Częstochowa, Poland, EU, domanski@imipkm.pcz.pl

Abstract

This study describes modelling of the processes of steel hardening. The first priority was given to thermal phenomena, phase transformations in solids and mechanical processes. The issue of heat conductivity was based on the equation of apparent thermal conductivity with an integrating factor. Numerical algorithms for kinetics of phase transformations and evaluation of fractions of phases were built on the diagrams of continuous heating and cooling of tool steel (CHT and CCT). The theoretical model of phase transformations was then verified by experiments. In modelling of mechanical phenomena, the equilibrium equations and constitutive relations were adopted in the rate form. Plastic deformations are determined by the theory of non-isothermal plastic flow associated with the von Misses yield criteria. The model assumed isotropic and kinematic hardening and stress/strain effects, thermal gradients, structural changes, plastic deformations and phase transformations were evaluated. Thermal and physical properties including the Young's modulus, shear modulus and elastic limit were directly dependent on temperature and steel phase composition. The issues of thermal strain elasticity were evaluated using the finite element method. Implemented algorithms were applied in computer stimulation of hardening of low-alloy tool steel. Numerical analysis of thermal effects and phase transformations, i.e. thermal stress and deformation in mechanical phenomena in a tool steel material undergoing hardening were made.

Keywords: phase transformations, stress, strain, hardening, transformations plasticity

1. INTRODUCTION

Since the tools are used in very different operating environments and conditions, steel must meet a wide variety of requirements, of which robustness is always the primary criterion to be achieved. To obtain the best steel properties, proper thermal processes including hardening and tempering are required. Currently, numerical methods are increasingly often used in modelling of technological processes. They allow to analyse the process as far as complex shapes are concerned and to stimulate different starting and boundary conditions. Further, numerical approach is very flexible, as both an extension of the numerical algorithm and measuring of the outcomes for varying different thermal and physical parameters that may be possible, are enabled. Quantitative evaluation of phase transformations, kinetics and analysis of the type of structure obtained as a result of cast steel cooling are required to calculate strains induced during the process. Current research of numerical modelling of heat processes tend to increase number of input parameters; in simulation of steel hardening, transformation deformations are also taken into account.

2. THERMAL PHENOMENA AND PHASE TRANSFORMATIONS

Temperature fields are obtained with solved of transient heat equation (Fourier equation) with source unit:

$$\nabla \cdot (\lambda \nabla(T)) - C\frac{\partial T}{\partial t} = -Q_v \tag{1}$$

where: $\lambda=\lambda(T)$ is the heat conductivity coefficient [W/(mK)], $C=C(T)=\rho(T)c(T)$ is effective heat coefficient, c - specific heat [J/(kgK)], ρ - thickness *[kg/m³]*, Q_v is intensity of internal source [W/m³] (this can also be the phase transformations heat).

In the model of phase transformations take advantage of diagrams of continuous heating (CHT) and cooling (CCT). In both case the phase fractions transformed during continuous heating (austenite) is calculated using the Johnson-Mehl and Avrami formula or modified Koistinen and Marburger formula (in relations on rate of heating):

$$\underline{\eta}_A(T,t)=1-\exp(-b(t_s,t_f)(t(T))^{n(t_s,t_f)}) \tag{2}$$

$$\eta_A^h(T,t)=1-\exp\left(-\left(\frac{T_{sA}-T}{T_{sA}-T_{fA}}\right)^m\right) \quad \text{for} \quad \dot{T}\geq 100\ K/s \tag{3}$$

where: $\underline{\eta}_A$ is austenite initial fraction nescent in heating process, T_{sA} is temperature of initial phase in austenite, T_{fA} - is final temperature this phase, m is a power index measured experimentally (it is *m = 2.5* for the investigated steel sample).

The coefficient $b(t_s,t_f)$ and $n(t_s,t_f)$ are obtain with (2) next assumption of initial fraction (η_s=0.01) and final fraction (η_f=0.99) and calculation are by formulas:

$$n(t_s,t_f)=\frac{\ln(\ln(0.01)/\ln(0.99))}{\ln(t_f/t_s)},\quad b(t_s,t_f)=\frac{-\ln(0.99)}{(t_s)^n} \tag{4}$$

Pearlite and bainite fraction (in the model of phase transformations upper and lower bainite is not distinguish) are determine by Johnson-Mehl and Avrami formula [1].

$$\eta_i(T,t)=\chi(1-\exp(-b(t(T))^n)) \tag{5}$$

The nascent fraction of martensite is calculated using the Koistinen and Marburger formula.

$$\eta_M(T)=\chi(1-\exp(-k(M_s-T))) \tag{6}$$

Increases of the isotropic deformation caused by changes of the temperature and phase transformation in the heating and cooling processes are calculated using the following relations [2,5]:

- heating

$$\dot{\varepsilon}^{Tph}=\sum_{k=1}^{k=5}\alpha_k\eta_k\dot{T}+\sum_{k=2}^{k=5}\varepsilon_k^{ph}\dot{\eta}_k \tag{7}$$

where $\alpha_k=\alpha_k(T)$ are coefficients of thermal expansion of: austenite, bainite, ferrite, martensite and pearlite, respectively, ε_A^{ph} (ε_1^{ph}) is the isotropic deformation accompanying transformation of the input structure into austenite, whereas ε_k^{ph} are isotropic deformations from phase transformation of: austenite into bainite, ferrite, martensite, or of austenite into pearlite, respectively.

The results of test simulations are shown in **Figs. 1÷6**. As no considerable structural changes have been observed as far as cooling rate was concerned (10÷30 K/s), only the results for 30 K/s are included. No material structural changes have been found for cooling rates 100 and 200 K/s, either, and thus only the results for the cooling rates100 and 300 K/s are shown.

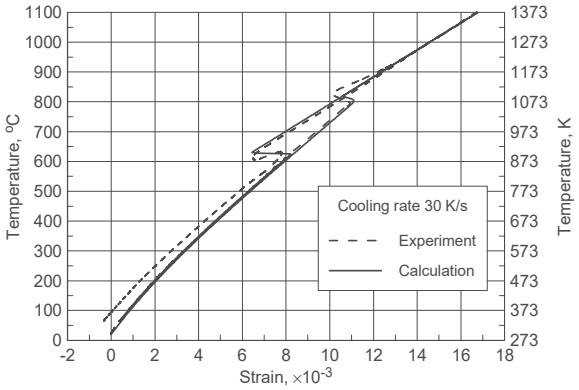

Fig. 1 Experimental and simulation dilatometric curves, cooling rate 30 K/s

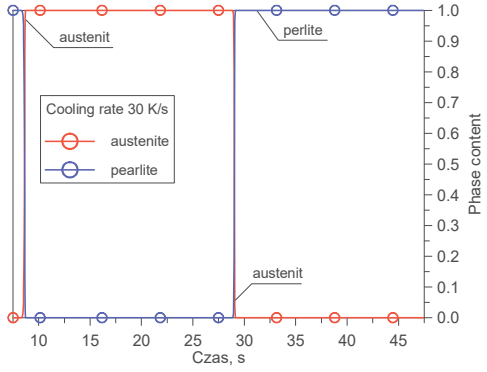

Fig. 2 Kinetics of transformations, cooling rate 30 K/s

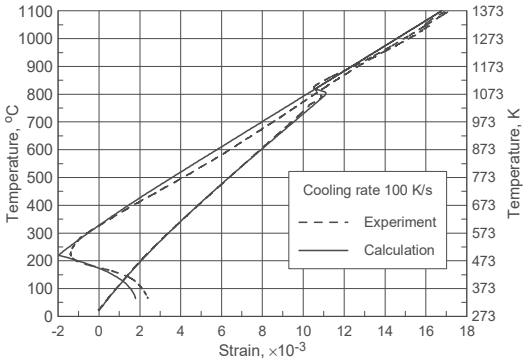

Fig. 3 Experimental and simulation dilatometric curves, cooling rate 100 K/s

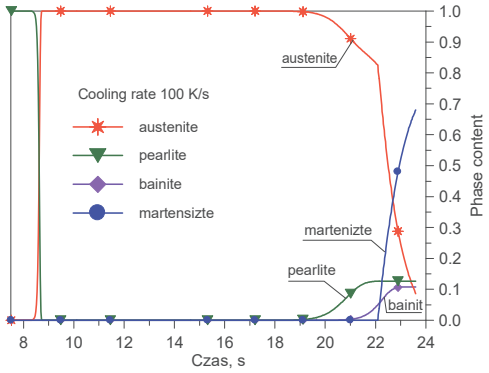

Fig. 4 Kinetics of transformations, cooling rate 100 K/s

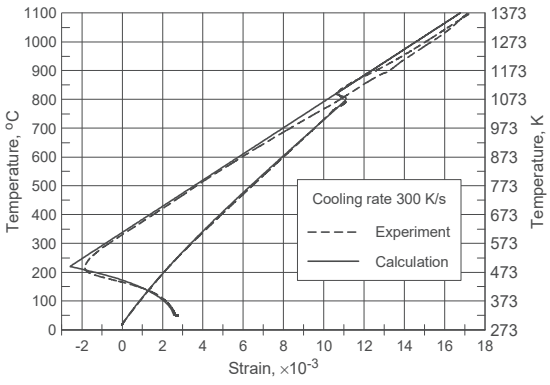

Fig. 5 Experimental and simulation dilatometric curves, cooling rate 300 K/s

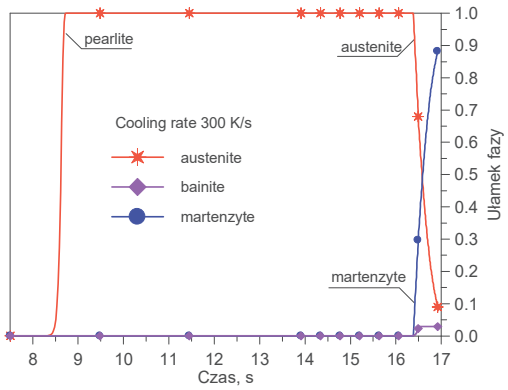

Fig. 6 Kinetics of transformations, cooling rate 300 K/s

An analysis of the test results revealed that the steel sample had pearlitic structure at slow cooling rates (**Fig. 1 and 2**). The volume fraction of pearlite decreases with increase of cooling rate whereas bainite content proportionally increases. A fast cooling rate will have the result of making the microstructure of steel of martensitic/bainitic or martensitic type (**Fig. 3 ÷ 4**). Hardly any diffusion transformations are shown on a dilatometric curve obtained from cooling a steel sample at a rate of 100 K/s (**Fig. 5 and 6**) within upper range of temperatures (only minor transformations); austenite decomposes into bainite (at a temperature above ~300 °C) and then into martensite (starting from Ms temperature). Further increase of the cooling rate maximizes

the martensite fraction in a steel sample. Cooling rate of 300 K/s increased the percentage of martensite to ~90, whereas the remaining ~10% comprised of residual austenite. On the basis of an analysis of simulation and dilatometric curves, the values of the thermal expansion coefficient (α_k) and isotropic structural deformations of each structural component $\left(\varepsilon_k^{ph}\right)$ were specified. These coefficients are: 22, 10, 14.5, 10 and 14.5 ($\times 10^{-6}$) [1/K] and 1.0, 4.5, 1.5, 8.7 and 1.5 ($\times 10^{-3}$) [3]. It was adopted that 1,2,3,4 and 5 refer to austenite, bainite, ferrite, martensite and pearlite, respectively. Coefficient of thermal expansion the pearlite structure for considered steel is dependent on temperature, approximate this coefficient by square function.

$$\alpha_{FP}(T) = -1.2955 \times 10^{-11} T^2 + 2.5232 \times 10^{-8} T + 3.7193 \cdot 10^{-6} \tag{8}$$

Analyses results from the model notice, are advantageously use in modelling of phase transformations the CCT graph for considered group steel. Accuracy results, particularly in range rate cooling are obtain, were for matrix formed with bainite.

3. MECHANICAL PHENOMENA

In modelling of mechanical phenomena, the equations for the equilibrium model were adopted as a rate-based approach. This, for example, enabled to track thermal and physical changes depending on temperature and phase composition with increased loading.

$$\nabla \circ \dot{\boldsymbol{\sigma}}(\mathbf{x},t) = \mathbf{0}, \quad \dot{\boldsymbol{\sigma}} = \dot{\boldsymbol{\sigma}}^T \tag{9}$$

where $\sigma=\sigma(\sigma_{\alpha\beta})$ is a strain tensor, symbol (°) means incomplete inner multiplication factor, $x=x(x_\alpha)$ represents a vector function of the position of the particle (point).

The equations are supplemented by constitutive relationships that, if based on an additive model of the rate of deformations, will be expressed as follows [4]:

$$\dot{\boldsymbol{\sigma}} = \mathbf{E} \circ \left(\dot{\boldsymbol{\varepsilon}} - \dot{\boldsymbol{\varepsilon}}^{Tph} - \dot{\boldsymbol{\varepsilon}}^{p} - \dot{\boldsymbol{\varepsilon}}^{tp}\right) + \dot{\mathbf{E}} \circ \boldsymbol{\varepsilon}^{e} \tag{10}$$

where: $E=E(T, \Sigma\eta_k)$ is a strain tensor dependent on temperature (T) and phase composition $(\Sigma\eta_k)$, εe represents an tensile deformation tensor, ε_{Tph} - isotropic tensor of thermal and structural deformations, ε^p - plastic deformation tensor, whereas ε_{tp} represents a tensor of transformation deformations.

There is a linear dependence of thermal and physical parameters contained in material constant tensor (E), for example Young's modulus (E) and static modulus (E_t) and the temperature and phase composition:

$$E\left(T, \sum \eta_k\right) = \sum E_k(T)\eta_k, \quad E_t\left(T, \sum \eta_k\right) = \sum E_{tk}(T)\eta_k, \quad k = 1,...,5 \tag{11}$$

where η_k is a fraction of k-phase in the steel structure.

Plastic deformations are determined using the theory of non-isothermal plastic flow associated with the von Misses yield criteria and isotropic or kinematic hardening. Thus, plastic flow functions $(f=f(\sigma,Y))$ are adopted as the following equations [5]:

$$f = \sigma_{ef} - Y\left(T, \sum \eta_k, \varepsilon_{ef}^{p}\right) = 0, \quad f = \sigma_{ef} - Y_0\left(T, \sum \eta_k\right) = 0 \tag{12}$$

where σ_{ef} represents an effective plastic strain, ε_{ef}^{p} - effective plastic deformation, $Y=Y(T,\Sigma\eta k, \varepsilon_{ef}^{p})$ is a yield strain improving plasticity of steel with composition of phases: $\Sigma\eta_k$ at a temperature T and plasticity factor ε_{ef}^{p}, and $Y_0=Y_0(T,\Sigma\eta_k)$ is a boundary of plasticity.

In high-strength anisotropic (kinematic) steel models, the rate of plasticity boundary changes are calculated using the following equation:

$$\dot{Y}_0 = \frac{\partial Y_0\left(T, \sum \eta_k\right)}{\partial T}\dot{T} + \sum_k \frac{\partial Y_0\left(T, \sum \eta_k\right)}{\partial \eta_k}\dot{\eta}_k == \kappa^T \dot{T} + \sum_k \kappa^{\eta_k}\dot{\eta}_k \tag{13}$$

In an iterative process of evaluation of plastic deformations, a modified Newton-Raphson algorithm is used.

4. EXAMPLE OF CALCULATIONS

Computer software intended for simulation of hardening phenomena was developed using the hardening models presented above. The software was then applied for direct numerical simulations of hardening of a carbon steel sample C80U. The starting microstructure of the sample was of pearlitic type (spheroidite). Simulation was run after partial austenitisation (surface hardening). An axially symmetric sample measuring ϕ 25×50 mm underwent a hardening simulation. The sample was heated using a boundary condition consistent with Newton's law, simulating heating in a fluid carrying heat at a temperature of 1550 K. Starting temperature of the sample that had a pearlitic (spheroidite) structure, was 300 K. The coefficient of heat transfer from fluid heating medium was constant (not dependent on temperature) and was 3800 W/(m^{2}K). On frontal surfaces of the sample, a lower coefficient of heat transfer of 2000 W/(m^{2}K) was adopted, thus taking into account a considerably lower index of circulation of the heating medium over the frontal surfaces of heated steel (decreased in real-life conditions). Simulation of heating was continued until a maximum temperature of 1350 K around point 3 was reached. In simulation of heating phase transformation (transformation of austenite), CHT diagram was applied, using $A_{c1}(t)$, $A_{ccm}(t)$. Temperature distribution and austenite phase obtained after completion of heat treatment are presented in **Fig. 7**.

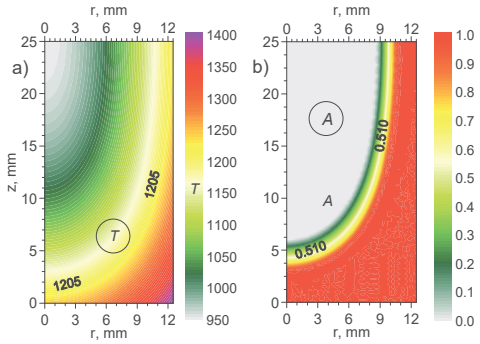

Fig.7 After-heating distribution of a) temperature [K], b) austenite,

Distribution of phases after hardening completion is shown in **Fig. 7**, whereas a comparison of zones after cooling in highlighted points are presented in **Fig. 8**.

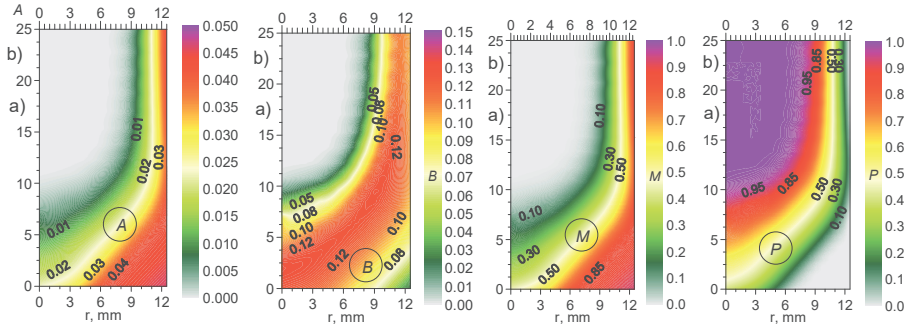

Fig.8 Distribution of phase volume fractions after cooling: a) austenite, b) bainite, c) martensite, d) perllite

Internal lattice strain distribution after quenching is shown in **Fig. 8**. In column a) the results of the model in which isotropic hardening was assumed are presented, in b) - results of the model with kinematic hardening assumed.

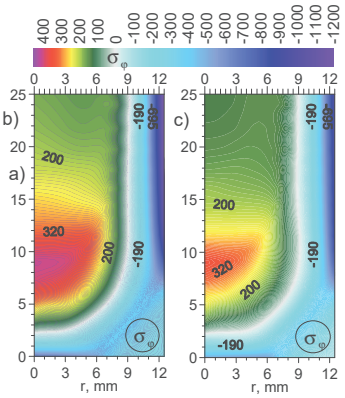

Fig.9 Distribution of circumferential residual stress

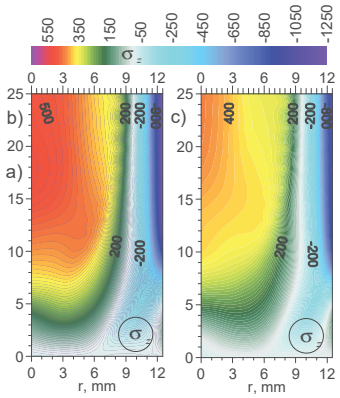

Fig.10 Distribution of axial residual stress

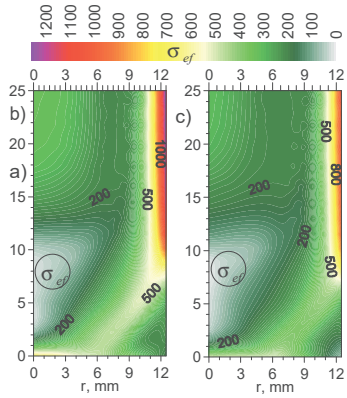

Fig.11 Distribution of effective residual stress

CONCLUSIONS

The austenite zone obtained from steel heating with parameters adopted in the simulation is very advantageous before the phase of cooling (**Fig. 7**). Surface layers are composed of pure austenite which results in a very advantageous structural composition of the hardened zone after cooling. Martensite and residual austenite are found only in the surface layers whereas bainite is located more deeply. At this stage of simulation, the advantageous distribution of quenching stresses and valuable zone of steel reinforcement can be already predicted. Distributions of stresses are similar in both models of either isotropic or kinetic strengthening and thus their values can be adopted as comparable. In both cases, distributions of considerable normal quenching stresses are favourable. In kinematic strengthening model, the level of normal and effective strains was mildly lower. This can be also analyzed by tracking the generation of quenching strains. The pattern of distribution of plastic deformations are also comparable, however, distribution of transformation deformation in case of isotropic strengthening slightly differs from the model of kinetic strengthening. The differences between the results obtained from each type of simulation of mechanical phenomena depending on the type of reinforcing of the steel sample are directly associated with the selection of quenching method. Simulation of heating and cooling shows that during quenching of steel, both enhancement and relieving of stress occur (**Figs. 9-11**). Distributions of effective deformations are advantageous, as well. The sample was reinforced in the surface layers, which means that as a result of this type of hardening, steel material acquires good mechanical properties in outer layers (increased boundary of plasticity).

REFERENCES

[1] OLIVEIRA W.P, SAVI M.A., PACHECO P.M.C.L., SOUZA L.F.G., Thermomechanical analysis of steel cylinders with diffusional and non-diffusional phase transformations. *Mechanics of Mate.,* 42, 2010, 31-43.

[2] KANG S.H., IM Y.T., Thermo-elesto-plastic finite element analysis of quenching process of carbon steel. *Int. J. Mech. Sci.*, 49, 2007, 13-16.

[3] BOKOTA A., DOMAŃSKI T., Numerical analysis of thermo-mechanical phenomena of hardening process of elements made of carbon steel C80U*, Arch. Metall. Mater.*, 52, 2, 2007, 277-288.

[4] JU D.Y., ZHANG W.M., ZHANG Y., Modeling and experimental verification of martensitic transformation plastic behavior in carbon steel for quenching process, *Mater. Sci. Eng.,* A 438-440, 2006, 246-250.

[5] LEE K.J., Characteristics of heat generation during transformation in carbon steel. Scr. Mater., 40, 1999 735-742.